Journal of Molecular Liquids 226 (2017) 2–8

Contents lists available at ScienceDirect

Journal of Molecular Liquids

journal homepage: www.elsevier.com/locate/molliq

A joint experimental and computational study on ethylammonium nitrate-ethylene glycol 1:1 mixture. Structural, kinetic, dynamic and spectroscopic properties

Alessandro Mariani [a,*], Marco Campetella [b], Claudia Fasolato [c,d], Maddalena Daniele [e], Francesco Capitani [c], Luigi Bencivenni [a], Paolo Postorino [c], Stefano Lupi [e], Ruggero Caminiti [a,f], Lorenzo Gontrani [a]

[a] Dipartimento di Chimica, La Sapienza Università di Roma, P. le A. Moro 5, 00185 Roma, Italy
[b] Dipartimento di Chimica e Chimica Industriale, Università di Pisa, Via G. Moruzzi 13, 56126, Pisa, Italy
[c] Dipartimento di Fisica, La Sapienza Università di Roma, P. le A. Moro 5, 00185 Roma, Italy
[d] Center for Life Nanoscience, Istituto Italiano di Tecnologia, V. le Regina Elena 291, 00161 Roma, Italy
[e] Dipartimento di Fisica, Istituto Officina dei Materiali – CNR, La Sapienza Università di Roma, P. le A. Moro 5, 00185 Roma, Italy
[f] Centro di Ricerca per le Nanotecnologie Applicate all'Ingegneria, Laboratorio per le Nanotecnologie e le Nanoscienze, La Sapienza Università di Roma, P.le A. Moro 5, 00185 Roma, Italy

ARTICLE INFO

Article history:
Received 28 January 2016
Received in revised form 9 August 2016
Accepted 13 August 2016
Available online 16 August 2016

Keywords:
Ionic liquids
Binary mixture
Wide angle X-ray scattering
Spectroscopy
Computational simulations

ABSTRACT

The intrinsic molecular polarity of a molecule, *i.e.* its dipole moment, seems to have an important role in the mixing process of an Ionic Liquid and a Molecular Liquid. In this work we report a complete study on the overall organization of a 1:1 binary mixture of Ethylammonium Nitrate and Ethylene Glycol by means of Wide Angle X-Ray Scattering, Raman Spectroscopy and Far Infrared Spectroscopy. The interpretation of all the experimental data was aided by a variety of computational models obtained *via* Classical Molecular Dynamics, *ab initio* Molecular Dynamics and DFT calculations. We observe that in the samples examined the Nitrate anion is strongly solvated by glycol molecules. This interaction has notable consequences on experimental observations.

1. Introduction

The wide potential application of Ionic Liquids (ILs) has a strong appealing in both academy [1] and industry [2,3]. Their characteristic bulk molecular organization [4–7] leads to unique properties that can be tuned by chemical substitutions on the cation and/or the anion [8–10]. The possibility of doing so gave them the fame of "task specific solvents" [11–13]. If within the cation molecular structure is present an available proton (*i.e.* an exchangeable one), then the compound belongs to the class of Protic Ionic Liquids (PILs) [14,15]. Among them, Ethylammonium Nitrate (EAN) was the first ever reported room temperature IL [16] and its extensive 3D hydrogen bond network is fairly similar to the one of liquid water [17]. Moreover, EAN and water share quite a lot of properties, both as neat compounds and as mixed with other chemicals [18–25]. These two facts make EAN the perfect prototype to find general behaviours in PILs. Mixing of two components can be conveniently used to tune chemical and physical properties [26,27] avoiding an expensive and time-consuming *ad hoc* synthesis. Different functional groups on the molecular co-solvent may have a variety of consequences on structure, kinetics and the spectroscopic properties of the resulting mixture. It is possible to find a wide literature on EAN:co-solvent mixtures in which water [22], alcohols [28], DMSO [24], and other organic compounds [29,30] are involved. In this work we have chosen Ethylene Glycol because of its dipole moment value, which falls in the middle of the values of some other co-solvents studied (see Table 1). Fig. 1 shows a schematic representation of the molecules discussed in this work.

2. Material and methods

EAN was purchased from IoLiTec with a nominal purity of 99.8%. Excess water was removed by pumping the compound under high vacuum and slight heating (45 °C) overnight. The final amount of water was checked *via* ^{1}H NMR and it was undetectable (<0.02%). Ethylene Glycol was purchased from Sigma Aldrich at the highest available purity (≥99.8%) and used without further treatment. The 1:1 mixture was obtained by weighting the two neat compounds, followed by their mixing. For the Wide Angle X-Ray Scattering (WAXS) experiments the mixture, as well as the neat precursors, was injected into a 2 mm o.d. sealed quartz capillary. The scattering patterns were collected by a Bruker D8 Advance with DaVinci design diffractometer located at CNIS - La Sapienza University of Rome.

* Corresponding author.
E-mail address: alessandro.mariani@uniroma1.it (A. Mariani).

http://dx.doi.org/10.1016/j.molliq.2016.08.043
0167-7322/

Table 1
Dipole moments of some molecules of interest.

Water	Ethanol	Ethylene Glycol	Methanol	DMSO
1.52 Debye	1.66 Debye	2.27 Debye	2.87 Debye	4.10 Debye

The angle dispersive instrument is equipped with a Mo K_αX-Ray tube ($\lambda = 0.7107$ Å), whose radiation was focused onto the sample with Göbel mirrors. The 2θ angle range available was 2.75–142° with a step of 0.25° within Bragg-Brentano para-focusing geometry. The scattered intensity was gathered with the Lynxeye XE Energy-Dispersive 1-D detector.

The Far Infrared (FIR) spectra were collected through a Bruker 66 V Michelson interferometer equipped with a 3 μm thick Mylar beamsplitter and a Pyroelectric detector. The spectral resolution was 4 cm^{-1} and we cover the spectral region between 50 and 700 cm^{-1}. The liquid mixture was contained in an optical cell closed by polyetilene windows. The absorption coefficient was calculated through the equation $A = -\ln[\frac{I(\nu)}{I_0(\nu)}]$, where I ($I_0$) is the transmitted light intensity from the fill (empty) cell and ν is the frequency.

The Raman measurements were performed using a HR-Evolution microspectrometer (Horiba – Jobin Yvon), equipped with a 15 mW (10 mW on sample) He-Ne laser (632.8 nm wavelength). A 20× objective (n.a. 0.35) was used for the acquisition, in the backscattering geometry. The elastically scattered light was removed by a state-of-the-art optical filtering device based on three BragGrate notch filters and a charge-coupled-device (CCD) was used to collect the spectrum of the scattered radiation. The use of 600 lines/mm diffraction grating with 800 mm focal length ensured a spectral resolution better than 3 cm^{-1}. The frequencies were calibrated using the emission lines of a Neon lamp. The spectra were elaborated and analysed using Origin Pro 8.1 software (OriginLab, Northampton, MA).

2.1. Computational Methods

Several different simulations were carried out on this system to achieve the most complete scenario. The structure factor was modelled by Classical Molecular Dynamics following the scheme:

1. Generation of a simulation box containing the appropriate number of each molecular species in a random configuration. This was achieved using Packmol [31].
2. Energy minimization through 10^7 cycles at 0 K.
3. Heating the system at 50 K for 20 ps (timestep 1 fs) in an NVT *ensemble*.
4. NPT equilibration at 300 K and 1 bar for 5 ns (timestep 2 fs)
5. NVT equilibration at 300 K for 5 ns (timestep 2 fs)
6. NVT productive run at 300 K for 2 ns (timestep 2 fs)

To compute dynamic and kinetic properties, we added a further NVT productive phase at 300 K, simulating 37.5 ps with a timestep of 0.5 fs. All the classical simulations were carried out with AMBER12 [32]using the GAFF force field [33]. Missing parameters such as atom charges for ionic species were computed with the RESP fitting of the electrostatic potential at B3LYP/6-311++G** level of theory. A dielectric constant of 1.8 was employed for the calculation of electrostatic interactions in both simulations, since we observed [34] that this value gives the best reproducibility of the experimental density for neat EAN and for other

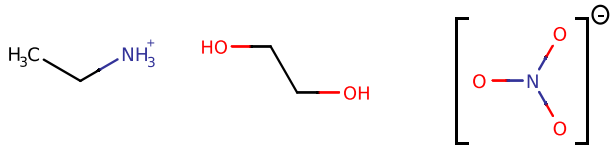

Fig. 1. Schematic representation of the molecules in this work.

Table 2
Number of molecules for each simulation carried out in this work.

Simulation	Neat glycol	1:1 mixture		Neat EAN
	Diol	IL	Diol	IL
Classical Dynamics (slow)	1000	600	600	1000
Classical Dynamics (fast)	500	250	250	500
ab initio Dynamics	10	4	4	6
DFT calculation	4	2	2	2

PILs. That is equivalent to scaling the atomic charges by a factor of ~0.75. The trajectories obtained in this way were therefore analysed using the TRAVIS software [35]. Raman spectra assignment was accomplished by *ab initio* molecular dynamics simulations. For all the systems, a pre-equilibration was performed employing Classical Molecular Dynamics within periodic boundary conditions, using AMBER12 [32] program package and the GAFF force field [33]. The simulations reproduce 2 ns of physical time at 300 K. The starting configurations resulting from this procedure were used to set up *ab initio* molecular dynamics simulations with the program package CP2k [36], using the Quickstep module [37] and orbital transformation [38] for faster convergence. The electronic structure was calculated at the level DFT, utilizing the PBE [39,40] functional, with the explicit Van der Waals terms including empirical dispersion correction (D3) from Grimme [41]. The MOLOPT-DZVP-SR-GTH [42] basis set and GTH pseudopotentials [43] were chosen. The time step was chosen to be 0.5 fs. The temperature was set at 300 K by a Nose-Hoover chain thermostat. After 7 ps of QM-equilibration, NVT trajectories of 30 ps were performed.

FIR spectra were interpreted through DFT calculations at B3LYP/6–311++G** level of theory performed with Gaussian-09 (D1) [44]. The number of fragments in each simulation is reported in Table 2. Classical Molecular Dynamics and the DFT calculations were run on the NARTEN cluster at the Chemistry Department of La Sapienza University of Rome. *ab initio* Molecular Dynamics was run on the cluster of the University of Pisa.

3. Results and discussion

WAXS patterns for the three samples in this work are reported in Fig. 2.

The agreement between the computed and experimental structure function is indeed satisfactory especially for the 1:1 binary mixture (herein after EGE5) and for neat Ethylene Glycol (EG). Mesoscopic heterogeneity is a well known feature of ILs [45,6,7], and PILs in particular show the relative "Low q Peak" (LqP) even when the alkyl tail is just two-carbon long, like in EAN [46,5,47]. It appears evident that the addition of glycol to EAN shifts the LqP at lower q values, from 6.7 nm^{-1} to

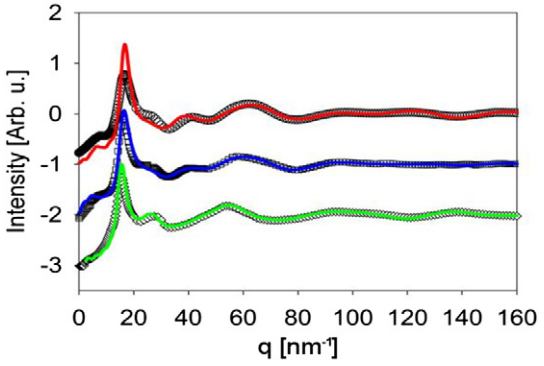

Fig. 2. Wide Angle X-Ray Scattering patterns collected at room conditions. Symbols are for experimental, lines for theoretical models. EAN (red); EAN:Ethylene Glycol 1:1 mixture (blue); Ethylene Glycol (green). Curves are vertically shifted for sake of clarity.

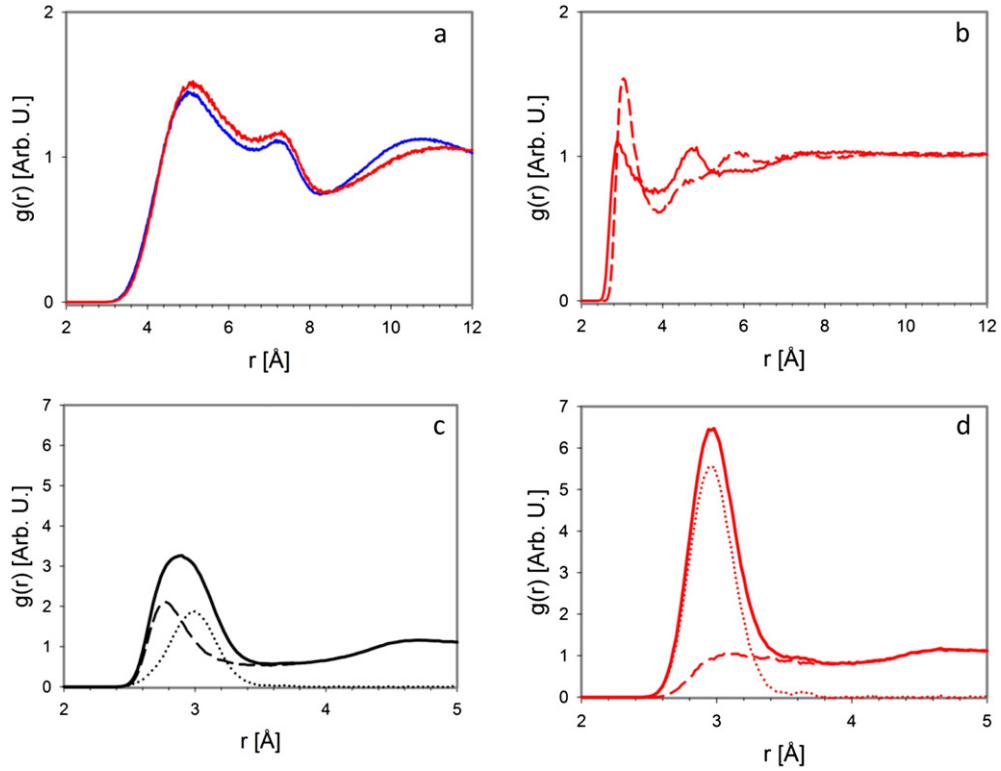

Fig. 3. Pair Distribution Functions of interest. (a) Nitrate-Nitrate (centre of masses), EAN (blue), EGE5 (red); (b) Nitrate-Glycol (Oxygen-Oxygen) (solid line), Ethylammonium-Glycol (Nitrogen-Oxygen) (dashed line), in EGE5; (c) Glycol-Glycol (Oxygen-Oxygen) intermolecular (dashed line), intramolecular (dotted line), total (solid line), in EG; (d) Glycol-Glycol (Oxygen-Oxygen) intermolecular (dashed line), intramolecular (dotted line), total (solid line), in EGE5.

5.7 nm^{-1}. It has been demonstrated that the LqP position is determined by Anion-Anion interactions [48], *via* the dimension of the apolar domain in the IL. Therefore, the glycol effect may be explained in two ways: 1) glycol is accommodated into the apolar domain of the PIL, enlarging it. 2) nitrate anions preferentially interact with glycol in the polar domain. This leads to a weaker interaction with the cations and, as a consequence, two nitrates are placed more distant. Ethylene Glycol is of course a polar molecule, so the first explanation is very unlikely, but it cannot be discarded on a qualitative basis. The LqP shift is exactly the same reported by Greaves et al. [28] for EAN:Ethanol 2:3 mixture. They explained the shift in terms of our first hypothesis. Ethanol is certainly similar to Ethylene Glycol, but the latter one has not an alkyl portion as definite as Ethanol, so further analysis is required. First of all, we have examined some Pair Distribution Functions (PDFs), to check differences between mixed and unmixed states. In Fig. 3 the most significant PDFs are reported.

It can be seen in Fig. 3.a that the nitrate-nitrate centre of masses correlation is affected by the presence of glycol. In particular, the first peak that in neat EAN is at 5 Å is shifted to slightly higher distances and a value of 5.2 Å is found. The most important shift is on the third peak that in the unmixed state occurs at 10.7 Å, while the much higher value 11.6 Å is observed in EGE5. The PDF integral is the coordination number (CN). Some CNs of interest are reported in Table 3.

The CN relative to the nitrate-nitrate centre of mass PDF shows clearly that the correlation between two anions is much weaker in presence of glycol. At the same time it can be seen that the ammonium head of the cation is nearly fully coordinated by anions in pure EAN, while an average value of 2.3 anions for each cation is found in EGE5. The most interesting structural considerations can be done on glycol surroundings. Ethylene Glycol may establish an intra-molecular hydrogen bond and, in its pure state, the closed form is by far the predominant. In Fig. 3.c,d the overall correlation between the oxygens of glycol is decomposed into its intra-molecular and inter-molecular contributions. First of all, the position of the overall peak is shifted in EG from 2.88 Å to 2.96 Å in EGE5, indicating a weakening of the interaction, while its intensity is nearly doubled meaning that this correlation is more persistent. These are apparently two contrasting observations, but the deconvolution of this PDF into its contributions shows a clear picture. The intra-molecular correlation remains stable in its position at 3 Å, and the intensity rises, meaning that there are more glycol molecules in the closed form. On the other hand, the inter-molecular peak is almost completely absent in the EGE5 system, meaning that glycol molecules preferentially do not bond themselves. The CNs for those correlations behave similarly. The intra-molecular hydrogen bond CN is always exactly 1.00, as it is expected, while the CN for the inter-molecular correlation drops from 1.15 in EG to 0.33 in EGE5. At last, looking at Fig. 3.b, the correlation between the nitrate oxygens and the glycol ones is shorter than that between the ethylammonium nitrogen and the glycol oxygens showing the peak at 2.8 Å and 3.2 Å respectively. Moreover, a CN of 1.98 anions around a central glycol molecule is calculated while a number of just 0.61 cations can be found there. This picture shows an arrangement where the nitrate replaces the other glycol molecules in the glycol solvation shell, meanwhile inducing the closed conformation of the diol. To understand the overall molecular arrangement around a central glycol molecule, we have computed some Spatial Distribution Functions (SDFs) and the results are reported in Fig. 4.a,b.

Table 3
Coordination numbers for all the possible hydrogen bonds in the studied systems.

System	Anion-Cation	Anion-Anion	Glycol-Glycol		Glycol-Cation	Glycol-Anion
			Intra	Inter		
EAN	2.98	7.12	–	–	–	–
EGE5	2.30	4.96	1.00	0.33	0.61	1.98
EG	–	–	1.00	1.15	–	–

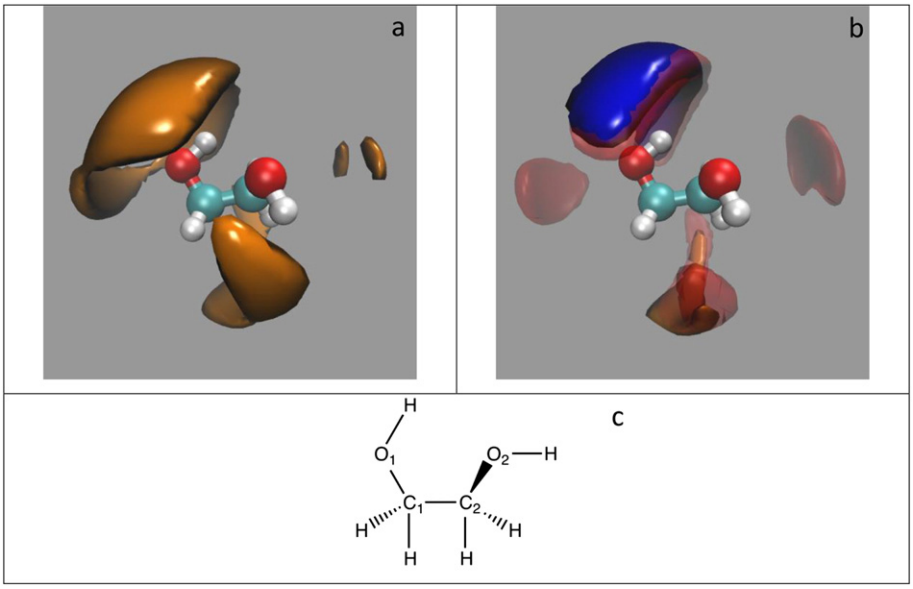

Fig. 4. (a) Spatial Distribution Function of the oxygens of the Ethylene Glycol around a central homologue molecule in EG; (b) Spatial Distribution Function of various atoms around a central glycol molecule in EGE5. Glycol oxygens (orange), Ethylammonium nitrogens (blue), Nitrate oxygens (red). (c) Schematic representation of Ethylene Glycol with atom labels.

For sake of clarity, we will refer to a certain atom according to the scheme in Fig. 4.c.

For EG (Fig. 4.a) other glycol molecules surround a central one preferentially near O_1 and under the plain defined by C_1, C_2 and O_2. Only a few molecules interact directly with O_2. In EGE5 the arrangement is quite different. Almost all the glycol molecules are replaced by nitrate anions that also interact with O_2 in the same way as with O_1. The cations are in competition with the anions for the interaction with O_1, but at longer distances. In Fig. 5 the situation around a central nitrate is shown.

In EAN (Fig. 5.a) other anions are equally disposed in equatorial and axial positions, while in EGE5 (Fig. 5.b) it is possible to observe a depletion of anions in equatorial position and a complete replacement of the axial ones by glycol molecules. Such a loss of correlation may be directly linked to the LqP shifting. To further understand the structural modifications, we have collected some vibrational spectra (Figs. 6 and 7). Raman and Infrared spectroscopies may be valuable tools in the determination of the intermolecular interactions. The collected spectra were interpreted with two different computational models and methods, namely Quantum Mechanics Molecular Dynamics (QMMD) for Raman, and DFT calculations for FIR.

The calculations were found to satisfactorily reproduce the experimental FIR and Raman spectra and the main conclusions may be summarized as follows:

(1) The highest measured, as well as computed, vibrational frequency is due to the OH stretching mode of the glycol molecule that is not involved in the hydrogen-bond network.
(2) The frequency of the NH stretching mode of the NH_3^+ group not involved in HB always occurs at lower frequency than the OH stretching.
(3) There is extended overlap between the hydrogen bonded OH and NH stretchings and the spectra show a broad band in correspondence of these modes. An attempted assignation was performed though careful data analysis and is presented in the following table (Table 4).
(4) The antisymmetric stretching of the nitrate group produces weak and broad Raman bands at 1373 and 1398 cm^{-1} for EAN and EGE5. The measured components of the degenerate $\boldsymbol{\nu_3}$ mode of the anion have the same splitting, namely 25 cm^{-1} revealing that the nitrogen-oxygen bonds interact with the surrounding

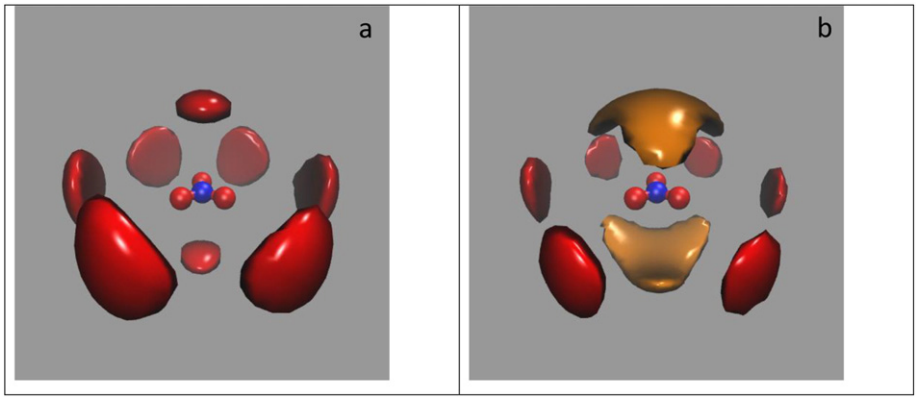

Fig. 5. Spatial Distribution Functions of various atoms around a central nitrate anion. Nitrate oxygens (red), Ethylene Glycol oxygens (orange). (a) EAN; (b) EGE5.

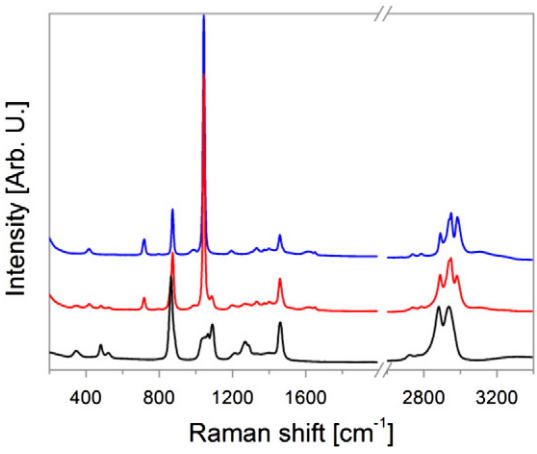

Fig. 6. Raman spectra of the systems in this work. EAN (blue); EGE5 (red); EG (black). Curves are vertically shifted for sake of clarity.

in a virtually identical way. The highest measured Raman band, closely lying around 1044 cm^{-1}, is assigned to the $\boldsymbol{\nu_1}$ symmetric stretching of the anion; this mode is actually unshifted upon changing the chemical composition of the sample.

(5) The remaining vibrations of the anion do not show either valuable shifts or splittings both in EAN and EGE5. The in-plane bending (the degenerate $\boldsymbol{\nu_4}$ mode) does not show any splitting due to degeneracy loss and is measured at 717 cm^{-1}; the out-of-plane bending (the $\boldsymbol{\nu_2}$ mode) is experimentally found at 829 cm^{-1}.

It is known that the vibrational bands associated to the asymmetric stretching nitrogen-oxygen of the nitrate anion exhibit a splitting of its two components when its surrounding is not perfectly isotropic. Under this consideration, there is an evident contrast between QMMD simulations and the B3LYP calculated vibrational spectra because QMMD method provides a larger value for the splitting of the $\boldsymbol{\nu_3}$ mode of the anion. In fact, the QMMD value ranging around 100 cm^{-1} contrasting an average value of 50 cm^{-1}. The overestimation observed in the former series of computations is due to difference existing between the number of anions not fully coordinated with respect to the number of anions completely coordinated. That is consequence of the reduced size of the model chosen for this analysis. This conclusion is supported from basilar geometrical considerations. If we consider the cluster to have a spherical shape, the ratio of the nitrate anions on the surface respect to the ones in the bulk, can be estimated by the Surface/Volume (S/V) ratio.

$$\begin{cases} S = 4\pi r^2 \\ V = \frac{4}{3}\pi r^3 \end{cases} \rightarrow \frac{S}{V} = \frac{3}{r}.$$

where r is the radius of the sphere. So the smaller the radius is (*i.e.* the fewer the molecules are) the more important the surface effects are. However, the computational cost of larger QMMD calculations makes it difficult to simulate much larger systems. Previous DFT calculations [49,50] performed on larger clusters suggest ~50 cm^{-1} as the best theoretical result for the splitting under consideration, in good agreement with the experimental findings reported in the present study. A general improvement, including to a more reliable description of the NH stretching vibrations, might be reached from B3LYP computations when larger clusters are taken into account. The interpretation of the vibrational spectra in the FIR region was accomplished using P.E.D. analysis provided from DFT calculations (equilibrium geometry, cartesian force constants and harmonic frequencies) employing a suitable internal coordinate set. Experimental spectra for the three systems are reported in Fig. 7.

Protic Ionic Liquids exhibit a peculiar band in this region at 120–210 wavenumbers. This is attributed at the interionic hydrogen bond stretching [15,17,51–56]. The effect of the co-solvent on the vibrational wavenumber of the said mode was determined by means of the frequency shifts reported in Table 5.

From the red shift of both components of the band, it is evident that hydrogen bond of the ion pair is weakened by the presence of glycol.

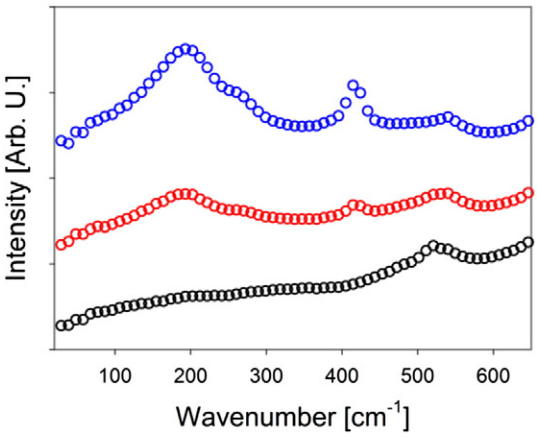

Fig. 7. Far Infrared spectra of the systems in this work. EAN (blue); EGE5 (red); EG (black). Curves are vertically shifted for sake of clarity.

Table 4
Raman spectra assignation for EAN and EGE5.

EAN			EGE5			
Raman Exp. [cm^{-1}]	QMMD [cm^{-1}]	B3LYP [cm^{-1}]	Raman Exp. [cm^{-1}]	QMMD [cm^{-1}]	B3LYP [cm^{-1}]	Description (EAN)
416.5	420	420	417.8	420	422	CCN bending
717.0	783	719	717.3		723	$\boldsymbol{\nu_4}$
829		835	829		834	$\boldsymbol{\nu_2}$
872.7		883	862.1/873.7			CN/CC stretching
1043.6	1035	1069	1043.7	1038	1080	$\boldsymbol{\nu_1}$
1194.3		1223	1196.9		1200	NH_3/CH_2 bendings
1221.8			1216.8			
1302.5			1289.6			
1331.7		1311	1332.5		1313	CH_2 bendings
1372.6	1321	1333	1372.8	1314	1376	$\boldsymbol{\nu_{3a}}$
1398.4	1423	1392	1399.0	1438	1420	$\boldsymbol{\nu_{3b}}$
1458.9		1499	1457.8		1499	CH_2 bendings
1476.1		1506	1466.1		1509	CH_2 bendings
1512.2		1519	1524.4		1517	CH_2 bendings
			1616.6		1633	NH_3^+ bendings
			1651.9		1696	NH_3^+ bendings
2786.0			2737.7			
2786.0			2785.5			
2890.6			2880.4/2888.2			CH stretching
2937.7			2938.4			CH stretching
2950.4			2950.6			CH stretching
2981.4			2980.0			CH stretching
2992.6			2991.4			CH stretching
3113.9			3108.6			NH stretching
3240.4			3220.5			NH stretching

Table 5
Far Infrared spectra assignation for EAN and EGE5.

EAN [cm^{-1}]	EGE5 [cm^{-1}]	Stretching Mode
165	134	interionic hydrogen bond s.s.
203	193	interionic hydrogen bond as.s.

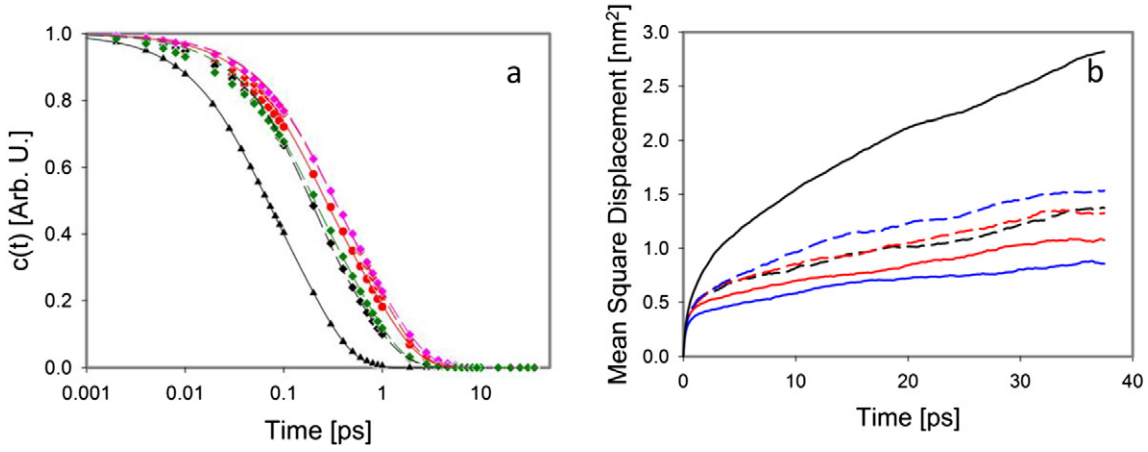

Fig. 8. (a) Continuous autocorrelation functions for all the possible inter molecular hydrogen bonds in the three studied systems. Symbols are for the data points, lines for the resulting fit. Glycol-glycol (black); ion pair (red); cation-glycol (green); anion-glycol (pink). EG (triangles); EGE5 (diamonds); EAN (circles); please note that the time is in logarithmic scale. (b) Mean square displacement for all the molecular species in the systems. Solid lines are for the neat compounds, dashed lines for EGE5. Glycol (black); anion (red); cation (blue).

Thereafter, H-Bonds lifetimes and self-diffusion were considered as a subject of our study. We used TRAVIS autocorrelation function tool to compute the hydrogen bonds lifetimes and the mean square displacement tool to obtain the self-diffusion functions. Fig. 8.a shows the autocorrelation function for all the possible inter-molecular hydrogen bonds.

The points obtained were fitted using the function:

$$C(t) = a{\cdot}e^{\frac{-t}{\tau_1}} + (1-a){\cdot}e^{\frac{-t}{\tau_2}}$$

where t is the time, a is a constant that determines the weight of the specific process, τ_1 and τ_2 are the characteristic time of the process 1 or 2 respectively. The process 1, which is fast, is the break of the hydrogen bond itself, while the slower process 2 is the migration of the fragments outside the solvent cage. As it can be seen from Table 6, the glycol-glycol hydrogen bond in EG is the fastest to break and glycol in EG is also the one with the fastest diffusion (Fig. 8.b). Those observations are explained in terms of the isoenergetic fast replacement of one broken hydrogen bond with a new one with another identical molecule in the system. From the values in Table 6, it can be said that in EGE5 the cation seems prefer to hydrogen bond an anion rather than a diol molecule. Here the coulombic forces play an important role in the selectivity. The most interesting observation that can be made is that the glycol-nitrate interaction is the most persistent one. This has a direct effect on the diffusion of both of them, in fact it appears evident from Fig. 8.b that the diffusions of nitrate and glycol are quite similar, meaning that the persistent hydrogen bond entangle the two particles during their motion. The a parameter is a qualitative probe of the strength of the hydrogen bond itself: if a has a value >0.5, then the interaction lifetime is dominated by the breaking up of the geometry (*i.e.* distance and angular conditions to have a hydrogen bond), otherwise the diffusion outside the solvent cage has a central role. In the former case the hydrogen bond is strong because the geometry breaking up is the kinetic relevant process. Looking at Table 6 it is possible to observe that hydrogen bond in the ionic couple is weaker in EGE5 than in EAN, while the strongest interaction is between glycol and the anion, confirming our interpretation.

Table 6
Fitting parameters for the autocorrelation functions of all the possible inter molecular hydrogen bonds in the systems studied.

System	Interaction	τ_1 [ps]	τ_2 [ps]	a
EAN	Ionic Pair	0.6785	5.1082	0.432484
EGE5	Ionic Pair	0.6043	5.9195	0.358108
	Glycol-Glycol	0.7474	3.1063	0.430837
	Ethylammonium-Glycol	0.4791	3.7430	0.404184
	Nitrate-Glycol	0.8444	6.2215	0.519356
EG	Glycol-Glycol	0.1363	1.2121	0.369162

4. Conclusions

Summarizing, in this work we have elucidated the role of Ethylene Glycol in the 1:1 binary mixture with the Protic Ionic Liquid Ethylammonium Nitrate. The glycol seizes the nitrate anions in order to establish strong and durable hydrogen bonds with them. Almost all the coordination sphere of the diol is constituted by anions and this phenomenon weakens the interaction with the ethylammonium, moving apart anions and cations. As a consequence, the nitrate-nitrate correlation is perturbed too, lending to the changes observed in the structure function. Raman and Far Infrared spectroscopies confirmed our structural picture. The characteristic FIR band of PILs at ~200 wavenumbers is shifted to smaller values in the mixture, suggesting a weakening of the ion pair's hydrogen bond. This has an effect even on the Raman spectra where it could be find that the band associated to the oop bending of the anion is red-shifted itself in the mixture, thus suggesting that nitrate is experiencing a different environment. Moreover, kinetic properties witness that the motion of the anion is entangled with the one of the glycol, confirming once more our overall picture of the system.

Acknowledgments

The authors thank CNIS (Research Centre for Nanotechnology applied to Engineering of La Sapienza University of Rome) for providing access to the D8 diffractometer and Prof. Ruggero Caminiti of Chemistry Department – La Sapienza University of Rome for granting us computing time on Narten Cluster. M. C. thank Prof. Benedetta Mennucci for granting computing time on the cluster of the University of Pisa.

References

[1] T. Greaves, C.J. Drummond, C. Chem. Rev. 115 (2015) 11379–11448.
[2] M.J. Earle, K.R. Seddon, Pure Appl. Chem. 72 (2000) 1391–1398.
[3] N.V. Plechkova, K.R. Seddon, Chem. Soc. Rev. 37 (2008) 123–150.
[4] E. Bodo, S. Mangialardo, F. Ramondo, F. Ceccacci, P. Postorino, J. Phys. Chem. B 116 (2012) 13878–13888.
[5] R. Hayes, S. Imberti, G.G. Warr, R. Atkin, Phys. Chem. Chem. Phys. 13 (2011) 3237–3247.
[6] O. Russina, A. Triolo, Faraday Discuss. 154 (154) (2012) 97–109.

[7] O. Russina, W. Schröer, A. Triolo, J. Mol. Liq. 210 (2015) 161–163.
[8] A. Triolo, O. Russina, R. Caminiti, H. Shirota, H.Y. Lee, C.S. Santos, N.S. Murthy, E.W. Castner, Chem. Commun. (Camb.) 48 (2012) 4959–4961.
[9] Y. Shen, D.F. Kennedy, T.L. Greaves, A. Weerawardena, R.J. Mulder, N. Kirby, G. Song, C.J. Drummond, Phys. Chem. Chem. Phys. 14 (2012) 7981–7992.
[10] M. Campetella, L. Gontrani, E. Bodo, F. Ceccacci, F.C. Marincola, R. Caminiti, J. Chem. Phys. 138 (2013) 184506.
[11] C. Yue, D. Fang, L. Liu, T.-F. Yi, J. Mol. Liq. 163 (2011) 99–121.
[12] Z.-Z. Yang, Y.-N. Zhao, L.-N. He, RSC Adv. 1 (2011) 545.
[13] Y. Kohno, H. Ohno, Chem. Commun. (Camb.) 48 (2012) 7119–7130.
[14] C.A. Angell, N. Byrne, J.-P. Belieres, Acc. Chem. Res. 40 (2007) 1228–1236.
[15] K. Fumino, A. Wulf, R. Ludwig, Phys. Chem. Chem. Phys. 11 (2009) 8790–8794.
[16] P. Walden, Bull. Acad. Imper. Sci St. Petersbg. 8 (1914) 405–422.
[17] K. Fumino, A. Wulf, R. Ludwig, Angew. Chem. Int. Ed. Eng. 48 (2009) 3184–3186.
[18] I. I. Vaismant, M. L. Berkowitz, 21 (1992), 1889–1896.
[19] S. Dixit, J. Crain, W.C.K. Poon, J.L. Finney, A.K. Soper, Nature 416 (2002) 829–832.
[20] B. Kirchner, M. Reiher, J. Am. Chem. Soc. 124 (2002) 6206–6215.
[21] L. Dougan, S.P. Bates, R. Hargreaves, J.P. Fox, J. Crain, J.L. Finney, V. Reat, A.K. Soper, J. Chem. Phys. 121 (2004) 6456–6462.
[22] R. Hayes, S. Imberti, G.G. Warr, R. Atkin, Angew. Chem. Int. Ed. Eng. 51 (2012) 7468–7471.
[23] O. Russina, A. Mariani, R. Caminiti, A. Triolo, J. Solut. Chem. 44 (2015) 685–699.
[24] O. Russina, M. Macchiagodena, B. Kirchner, A. Mariani, B. Aoun, M. Russina, R. Caminiti, A. Triolo, J. Non-Cryst. Solids 407 (2015) 333–338.
[25] A. Mariani, O. Russina, R. Caminiti, A. Triolo, J. Mol. Liq. 212 (2015) 947–956.
[26] A. Heintz, S.P. Verevkin, D. Ondo, J. Chem. Eng. Data 51 (2006) 434–437.
[27] H. Niedermeyer, J.P. Hallett, I.J. Villar-Garcia, P.a. Hunt, T. Welton, Chem. Soc. Rev. 41 (2012) 7780–7802.
[28] T.L. Greaves, D.F. Kennedy, N. Kirby, C.J. Drummond, Phys. Chem. Chem. Phys. 13 (2011) 13501–13509.
[29] R. Zarrougui, M. Dhahbi, J. Solut. Chem. 39 (2010) 1531–1548.
[30] B. Docampo-Álvarez, V. Gómez-González, T. Méndez-Morales, J. Carrete, J.R. Rodríguez, Ó. Cabeza, L.J. Gallego, L.M. Varela, J. Chem. Phys. 140 (2014) 214502.
[31] T.L. Greaves, D.F. Kennedy, N. Kirby, C. Drummond, Phys. Chem. Chem. Phys. 13 (30) (2011) 13501–13509.
[32] L. Martínez, R. Andrade, E.G. Birgin, J.M. Martínez, J. Comput. Chem. 30 (2009) 2157–2164.
[33] D.A. Case, T.E. Cheatham, T. Darden, H. Gohlke, R. Luo, K.M. Merz, A. Onufriev, C. Simmerling, B. Wang, R.J. Woods, J. Comput. Chem. 26 (2005) 1668–1688.
[34] J. Wang, R.M. Wolf, J.W. Caldwell, P.A. Kollman, D.A. Case, J. Comput. Chem. 25 (2004) 1157–1174.
[35] A. Mariani, R. Caminiti, M. Campetella, L. Gontrani, Phys. Chem. Chem. Phys. 17 (2015) 5298–5307.
[36] M. Brehm, B. Kirchner, J. Chem. Inf. Model. 51 (2011) 2007–2023.
[37] J. Hutter, M. Iannuzzi, F. Schiffmann, J. VandeVondele, Wiley Interdiscip. Rev. Comput. Mol. Sci. 4 (2014) 15–25.
[38] J. Vandevondele, M. Krack, F. Mohamed, M. Parrinello, T. Chassaing, J. Hutter, Comput. Phys. Commun. 167 (2005) 103–128.
[39] J. VandeVondele, J.J. Hutter, J. Chem. Phys. 118 (2003) 4365–4369.
[40] J.P. Perdew, K. Burke, M. Ernzerhof, D. of Physics, N. O. L. 70118 J. Quantum Theory Group Tulane University, Phys. Rev. Lett. 77 (1996) 3865–3868.
[41] J.P. Perdew, K. Burke, M. Ernzerhof, Phys. Rev. Lett. 78 (1997) 1396.
[42] S. Grimme, J. Comput. Chem. 27 (2006) 1787–1799.
[43] J. VandeVondele, J. Hutter, J. Chem. Phys. 127 (2007) 114105.
[44] S. Goedecker, M. Teter, J. Hutter, Phys. Rev. B 54 (1996) 1703–1710.
[45] M. J. Frisch, G. W. Trucks, H. B. Schlegel, G. E. Scuseria, M. A. Robb, J. R. Cheeseman, G. Scalmani, V. Barone, B. Mennucci, G. A. Petersson, H. Nakatsuji, M. Caricato, X. Li, H. P. Hratchian, A. F. Izmaylov, J. Bloino, G. Zheng, J. L. Sonnenberg, M. Hada, M. Ehara, R. Toyota, K. Fukuda, J. Hasegawa, M. Ishida, T. Nakajima, Y. Honda, O. Kitao, H. Nakai, T. Vreven, J. Montgomery, J. A., J. E. Peralta, F. Ogliaro, M. Bearpark, J. J. Heyd, E. Brothers, K. N. Kudin, V. N. Staroverov, R. Kobayashi, J. Normand, K. Raghavachari, A. Rendell, J. C. Burant, S. S. Iyengar, J. Tomasi, M. Cossi, N. Rega, M. J. Millam, M. Klene, J. E. Knox, J. B. Cross, V. Bakken, C. Adamo, J. Jaramillo, R. Gomperts, R. E. Stratmann, O. Yazyev, A. J. Austin, R. Cammi, C. Pomelli, J. W. Ochterski, R. L. Martin, K. Morokuma, V. G. Zakrzewski, G. A. Voth, P. Salvador, J. J. Dannenberg, S. Dapprich, A. D. Daniels, Ö. Farkas, J. B. Foresman, J. V. Ortiz, J. Cioslowski, D. J. Fox and I. Gaussian, 2009.
[46] O. Russina, A. Triolo, L. Gontrani, R. Caminiti, J. Phys. Chem. Lett. 3 (2012) 27–33.
[47] O. Russina, A. Triolo, Faraday Discuss. 154 (2012) 97–109.
[48] O. Russina, W. Schröer, A. Triolo, J. Mol. Liq. 210 (2015) 161–163.
[49] R. Atkinm, G.G. Warr, J. Phys. Chem. B 112 (2008) 4164–4166.
[50] R. Hayes, S. Imberti, G.G. Warr, Phys. Chem. Chem. Phys. 13 (2011) 3237–3247.
[51] J. Carrete, J. Vila, O. Cabeza, M. Turmine, L.M. Varela, S.B. Capelo, T. Méndez-Morales, J. Carrete, E. López Lago, J. Vila, O. Cabeza, J.R. Rodríguez, M. Turmine, L.M. Varela, J. Phys. Chem. B 116 (2012) 11302–11312.
[52] M. Campetella, L. Gontrani, F. Leonelli, L. Bencivenni, R. Caminiti, ChemPhysChem 16 (2015) 197–203.
[53] E. Bodo, P. Postorino, S. Mangialardo, G. Piacente, F. Ramondo, F. Bosi, P. Ballirano, R. Caminiti, J. Phys. Chem. B 115 (2011) 13149–13161.
[54] K. Fumino, V. Fossog, P. Stange, K. Wittler, W. Polet, R. Hempelmann, R. Ludwig, ChemPhysChem 15 (2014) 2604–2609.
[55] D. Paschek, B. Golub, R. Ludwig, Phys. Chem. Chem. Phys. 17 (2015) 8431–8440.
[56] R. Ludwig, Phys. Chem. Chem. Phys. 2015 (17) (2015) 13790–13793.